AIP | Applied Physics Letters

InGaAs heterostructure formation in catalyst-free GaAs nanopillars by selective-area metal-organic vapor phase epitaxy

J. N. Shapiro, A. Lin, P. S. Wong, A. C. Scofield, C. Tu, P. N. Senanayake, G. Mariani, B. L. Liang, and D. L. Huffaker

Citation: Applied Physics Letters **97**, 243102 (2010); doi: 10.1063/1.3526734
View online: http://dx.doi.org/10.1063/1.3526734
View Table of Contents: http://scitation.aip.org/content/aip/journal/apl/97/24?ver=pdfcov
Published by the AIP Publishing

InGaAs heterostructure formation in catalyst-free GaAs nanopillars by selective-area metal-organic vapor phase epitaxy

J. N. Shapiro,[a] A. Lin, P. S. Wong, A. C. Scofield, C. Tu, P. N. Senanayake, G. Mariani, B. L. Liang, and D. L. Huffaker[b]
Department of Electrical Engineering and California Nano-Systems Institute, University of California at Los Angeles, Los Angeles, California 90095, USA

(Received 21 August 2010; accepted 22 November 2010; published online 14 December 2010)

We investigate axial GaAs/InGaAs/GaAs heterostructures embedded in GaAs nanopillars via catalyst-free selective-area metal-organic chemical vapor deposition. Structural characterization by transmission electron microscopy with energy dispersive x-ray spectroscopy (EDS) indicates formation of axial $In_xGa_{1-x}As$ ($x \sim 0.20$) inserts with thicknesses from 36 to 220 nm with $\pm 10\%$ variation and graded Ga:In transitions controlled by In segregation. Using the heterointerfaces as markers, the vertical growth rate is determined to increase linearly during growth. Photoluminescence from 77 to 290 K and EDS suggest the presence of strain in the shortest inserts. This capability to control the formation of axial nanopillar heterostructures is crucial for optimized device integration. © *2010 American Institute of Physics*. [doi:10.1063/1.3526734]

With continued maturity of self-assembled synthesis processes, nanowires (NWs) are the subject of extensive studies in many semiconductor material systems for their small size, large surface to volume ratio, and applications in a large variety of devices. Nanowire-based device demonstrations include photovoltaics,[1] high speed transistors,[2] high sensitivity detectors,[3] and new types of emitters.[4,5] The conventional formation method is the vapor-liquid-solid (VLS) technique in which a metal catalyst enhances adatom incorporation at the catalyst/semiconductor interface to promote vertical growth. While the VLS technique allows for flexibility in material choices, the NW dimensions, location, and crystallographic orientation are difficult to control. Furthermore, there may be contamination from the catalysts[6] that can lead to leakage current in III-V NW-based devices.[7]

Patterned nanopillar (NP) formation by selective-area epitaxy (SAE) offers a catalyst-free approach that avoids contamination and, more importantly, offers the ability to grow large arrays of pillars with lithographically defined diameters and locations.[8] However, in the absence of a growth catalyst to promote vertical growth, adatom incorporation is determined by diffusion lengths and binding energies, and the crystal shape is determined by the relative surface energies of the crystal planes.[9]

Homoepitaxy of catalyst-free NPs has been studied in several III-V binary and ternary materials;[8] however, core-shell and axial heteroepitaxy are in their infancy using this growth mode. Core-shell heterostructures were demonstrated in GaAs/GaAsP,[10] GaAs/InAs,[11] and GaAs/AlGaAs,[12] but axial heterostructures have been elusive. Very thin axial InGaAs double heterostructures were reported in catalyst-free NPs,[13] but detailed measurement of indium content and heterointerfaces was not addressed. Recently InGaAs and GaSb axial heterostructures were reported in self-catalyzed NWs by VLS;[14,15] however, the liquid droplet promoting growth in the axial direction makes those growths considerably different than this work. In this work, we report on the controlled formation of axial GaAs/InGaAs/GaAs heterostructures of varied thickness grown by catalyst-free SAE metal-organic chemical vapor deposition (MOCVD). This capability is crucial for designing and realizing high-performance NP-based optoelectronic devices.

The axial GaAs/InGaAs/GaAs heterostructure NPs are grown on a patterned GaAs (111)B substrate via SAE. The SiO_2 growth mask is patterned into 200 μm square arrays of nanoholes (80 ± 5 nm diameter and 300 nm pitch) using electron beam lithography and reactive ion etching. The NP samples, including InGaAs inserts, are grown at 720 °C in a hydrogen environment at 60 Torr. The GaAs sections are grown using trimethyl-gallium (TMGa) and tertiary-butyl-arsine (TBA) with a V-III ratio of 9. The precursor flow rates result in 0.5 Å/s equivalent planar growth rate on GaAs (001) substrates. To form the axial InGaAs inserts, trimethyl-indium (TMIn) is introduced keeping TMGa unchanged at a molar flow ratio of 1:4 (TMIn:TMGa), and the V-III ratio is increased to 50. 30 s growth interrupts are included before and after formation of each insert to adjust the TBA flux. Three samples are studied including NPs with single inserts grown for 180 and 90 s and NPs with triple inserts grown for 60 s each and separated by GaAs segments grown for 120 s. Resulting insert thickness and composition are analyzed below.

Figure 1(a) shows a 45° tilted scanning electron microscope (SEM) image of a representative NP ensemble with 85 ± 8 nm diameter and lengths of 1.8 ± 0.08 μm. The inset shows a top-down image of the pillar tip with $\{01\bar{1}\}$ side facets. Figures 1(b) and 1(c) show high angle annular dark field (HAADF) scanning transmission electron micrographs (STEMs) of multiple wires with single InGaAs 90 s and 3×60 s InGaAs inserts, respectively. The InGaAs inserts, appear brighter compared to the surrounding GaAs. The length of inserts measured from multiple dark field STEMs are 220 ± 20 and 130 ± 10 nm from the 180 and 90 s growths, respectively. The 3×60 s inserts become progressively thicker from 36 ± 4 nm to 53 ± 4 nm and 62 ± 6 nm.

Figures 2(a) and 2(b) plot both In content and growth time versus position along a single representative 3×60 s and 90 s pillars, respectively. The pillar STEM image is shown to the left of each plot. The In content is measured

[a]Electronic mail: jns@ee.ucla.com.
[b]Electronic mail: huffaker@ee.ucla.edu.

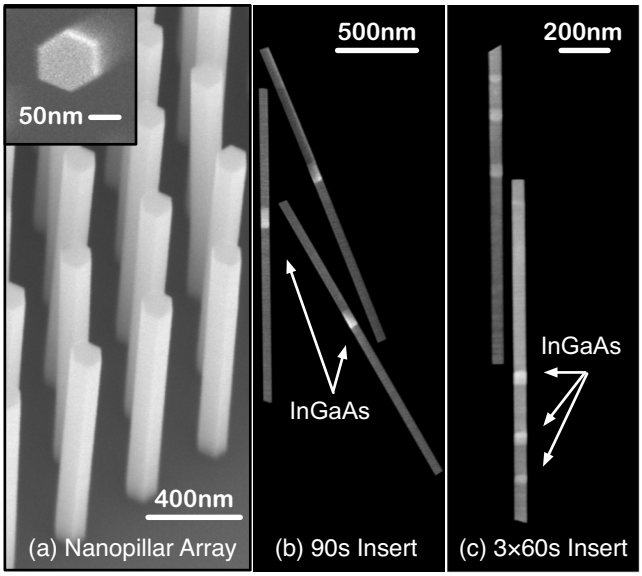

FIG. 1. (a) SEM side-angle image of nanopillar array with axial InGaAs inserts. The inset shows a plan view image of hexagonal NP cross section. (b) HAADF STEM of pillars with 90 s InGaAs inserts and (c) 3×60 s InGaAs inserts.

using line scan energy dispersive x-ray spectroscopy (EDS) with an ~1 nm spot size and 0.04 background noise levels. Peak In contents in the $In_xGa_{1-x}As$ alloy are x=0.21 and x =0.16 for the 180 and 90 s inserts, respectively. The three insets in the 3×60 s pillar have increasing In contents of x_1=0.13, x_2=0.16, and x_3=0.19, which we speculate is caused by cumulative strain along pillar length allowing more In to incorporate in subsequent inserts. Spikes in In content correspond to the bright segments in the adjacent STEM. The insets show magnified views of the inserts enclosed by a dashed box to elucidate In content at each heterointerface. Both insets show an initial rise in In to ~10% followed by a gradual increase to the respective peak value. Short period (<5 nm) intensity fluctuations visible in the high resolution STEM correspond to stacking faults visible in bright field TEM (not shown). We attribute the graded In:Ga at the bottom interface to In segregation as the growth front progresses.[16] The more abrupt In:Ga transition at the top interface is likely caused by strain-driven In:Ga intermixing, which occurs during the growth pause.

The vertical position of each InGaAs/GaAs heterointerface (open circles) marks a distinct point of time in the growth recipe and allows calculation of growth rate. The initial and final GaAs segments in all samples have 10 and 5 min durations, respectively. For the sample with triple inserts, the two intermediate segments were 2 min in duration each. In Figs. 2(a) and 2(b) the first 10 min of growth result in ~200 and ~800 nm of vertical growth, respectively. This discrepancy can be understood if the NP growth rate increases exponentially with time. Small variations early on in NP formation are amplified by the exponential dependence on time, resulting in large differences in height. Indeed, from Figs. 2(a) and 2(b), we observe that the GaAs segments get longer for equivalent or shorter growth times as the pillar grows indicating an increasing vertical growth rate. The slope of the dashed line connecting the heterointerface markers thus approximates the growth rate, which increases for each GaAs segment of pillar.

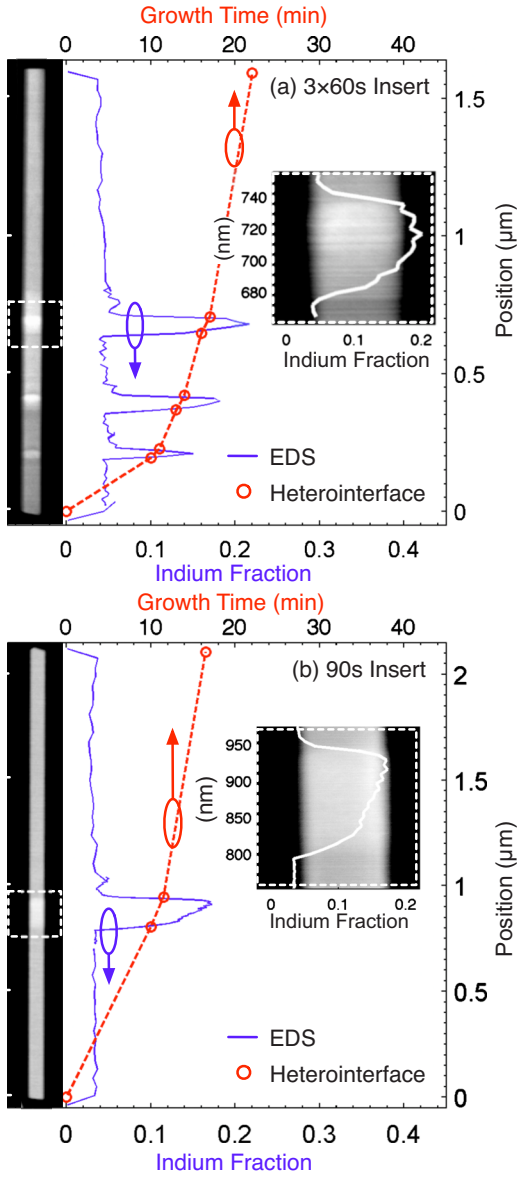

FIG. 2. (Color online) HAADF STEM, In content (solid) measured by EDS, and growth time (dashed) with (a) 3×60 s InGaAs inserts and (b) 90 s insert. (Insets) High resolution HAADF STEM and EDS revealing the In content variation along a single InGaAs insert indicated by a dashed box.

Figure 3 shows the approximate growth rate, (length/growth time) of each GaAs segment as a function of the vertical position of the segment midpoint. Data are collected for five wires from each sample. The dashed line is a linear fit to the data showing the vertical growth rate R_h increases with position h as R_h=0.26[nm/s]+2.38[nm/s μm]h. From Ref. 9, we explain this dependence by considering the possible sources of adatoms contributing to vertical pillar growth. In Eq. (1) we define an infinitesimal volume at the pillar tip $a^2\Delta h$, which grows in a time Δt where a represents pillar diameter; see Fig. 3 inset. The three sources of adatoms include direct incorporation from the vapor at the pillar tip, capture and subsequent adatom diffusion along the $\{01\bar{1}\}$ NP sidewalls, and capture on the SiO_2 mask area (s^2-a^2), expressed in the three terms below.

$$a^2\Delta h = [C_1a^2 + C_2 4ha + C_3(s^2 - a^2)]\Delta t. \quad (1)$$

The coefficients C_1, C_2, and C_3 account for the net effects of diffusion, adsorption, and desorption as the adatoms encoun-

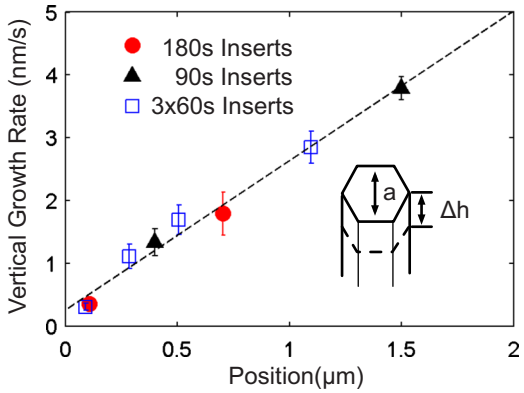

FIG. 3. (Color online) Markers show average growth rate for each GaAs pillar segment plotted vs the position of the segment midpoint. The dashed line is a linear least-squares fit to data showing that vertical growth rate increases linearly with position. The illustration depicts the volume of material deposited at the pillar tip as described in Eq. (1).

ter the crystal planes. When expressed as vertical growth rate R_h, Eq. (1) becomes

$$R_h = \frac{\Delta h}{\Delta t} = \left[C_1 + C_3\left(\frac{s^2}{a^2} - 1\right)\right] + \frac{4C_2}{a}h. \quad (2)$$

The term in square brackets varies with mask pitch s and pillar diameter a, which remain constant. The second term represents the vertical growth rate contribution from the pillar sidewalls.

The measured linear dependence of vertical growth rate on position reveals pillar sidewalls are the dominant source of adatoms driving midstage pillar growth for this pattern geometry. Adsorption directly from the vapor onto the pillar tip and the surrounding mask area are important effects at the early stages of pillar formation but eventually the pillar sidewalls contribute the majority of adatoms to the growing pillar tip.

Indium content and crystal quality are further verified by temperature-dependent microphotoluminesence (PL) of the samples with 180, 90, and 60 s inserts using a 0.5 m focal length spectrometer and an InGaAs focal-plane-array detector. The 659 nm, 0.5 mW diode pump laser is focused to ~3 μm spot to excite an ensemble of ~50 NPs. Figures 4(a) and 4(b) show a 77 K PL spectrum and PL peak wavelength versus temperature for all three samples. The 77 K emission peaks at a wavelength of 1021 nm for the 180 s insert and 1013 nm for the 90 s insert. The 3×60 s inserts have an emission peak at 988 nm and a shoulder at 932 nm. The full width at half maximum for all three samples is 70–80 nm at room temperature, decreasing to 35–40 nm at 77 K. In all cases the PL emission is consistent with an In content of 0.15–0.2 using published formulas for InGaAs bandgap at 77 K.[17] The slight blueshift from 180 to 90 s inserts is consistent with a reduced In content. A large blueshift from 90 to 60 s inserts despite equivalent In content is likely caused by increased strain in the shorter inserts.[18]

In summary, GaAs/InGaAs/GaAs axial double heterostructures embedded in GaAs patterned NPs have been grown by SAE MOCVD. Single pillars are studied by TEM and EDS to show the control of insert thickness and a variation of In content along the growth direction of the pillars. Examination of growth rates using the heterostructure interfaces as markers reveals a linear dependence of pillar growth rate on pillar height indicating that the entire sidewall of the pillar plays a role in midstage pillar growth. These types of quantum structures in single semiconductor nanopillars have the potential for application in electronics and optoelectronics.

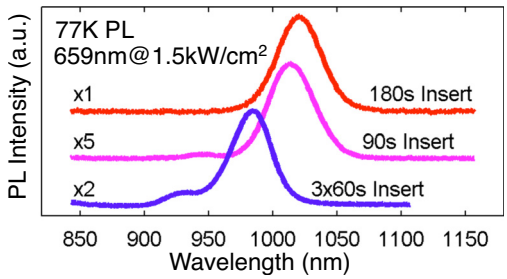

FIG. 4. (Color online) 77 K PL spectra of 180, 90, and 3×60 s samples normalized to illustrate blueshift of PL from pillars with shorter inserts.

The authors gratefully acknowledge the financial support by NSF (Grant No. ECCS-0824273), (Grant No. DMR-1007051), (Grant No. DGE-0903720), AFOSR (Grant No. FA9550-08-1-0198), (Grant No. FA9550-09-1-0270), and DoD (Grant No. NSSEFF N00244-09-1-0091). This work was performed in collaboration with Dr. Aaron Gin, at the Center for Integrated Nanotechnologies, U.S. Department of Energy, Office of Basic Energy Sciences (Contract No. DE-AC52-06NA25396) and Sandia National Laboratories (Contract No. DE-AC04-94AL85000).

[1]G. Mariani, R. B. Laghumavarapu, B. Tremolet de Villers, J. Shapiro, P. Senanayake, A. Lin, B. J. Schwartz, and D. L. Huffaker, Appl. Phys. Lett. **97**, 013107 (2010).
[2]S. A. Dayeh, D. P. R. Aplin, X. Zhou, P. K. L. Yu, E. T. Yu, and D. Wang, Small **3**, 2 (2006).
[3]C. Soci, A. Zhang, B. Xiang, S. A. Dayeh, D. P. R. Aplin, J. Park, X. Y. Bao, Y. H. Lo, and D. Wang, Nano Lett. **7**, 1003 (2007).
[4]S. D. Hersee, M. Fairchild, A. K. Rishinaramangalam, M. S. Ferdous, L. Zhang, P. M. Varangis, B. S. Swartzentruber, and A. A. Talin, Electron. Lett. **45**, 75 (2009).
[5]F. Qian, Y. Li, S. Gradeak, D. Wang, C. J. Barrelet, and C. M. Lieber, Nano Lett. **4**, 1975 (2004).
[6]D. E. Perea, J. E. Allen, S. J. May, B. W. Wessels, D. N. Seidman, and L. J. Lauhon, Nano Lett. **6**, 181 (2006).
[7]K. Haraguchi, K. Hiruma, T. Katsuyama, and T. Shimada, Curr. Appl. Phys. **6**, 10 (2006).
[8]J. Motohisa, J. Noborisaka, J. Takeda, M. Inari, and T. Fukui, J. Cryst. Growth **272**, 180 (2004).
[9]K. Ikejiri, T. Sato, H. Yoshida, K. Hiruma, J. Motohisa, S. Hara, and T. Fukui, Nanotechnology **19**, 265604 (2008).
[10]B. Hua, J. Motohisa, Y. Kobayashi, S. Hara, and T. Fukui, Nano Lett. **9**, 112 (2009).
[11]H. Paetzelt, V. Gottschalch, J. Bauer, G. Benndorf, and G. Wagner, J. Cryst. Growth **310**, 5093 (2008).
[12]K. Tomioka, Y. Kobayashi, J. Motohisa, S. Hara, and T. Fukui, Nanotechnology **20**, 145302 (2009).
[13]L. Yang, J. Motohisa, J. Takeda, K. Tomioka, and T. Fukui, Appl. Phys. Lett. **89**, 203110 (2006).
[14]S. Plissard, K. A. Dick, X. Wallart, and P. Caroff, Appl. Phys. Lett. **96**, 121901 (2010).
[15]M. Heiß, A. Gustafsson, S. Conesa-Boj, F. Peiro, J. R. Morante G. Abstreiter, J. Arbiol, L. Samuelson, and A. F. Morral, Nanotechnology **20**, 075603 (2009).
[16]K. Muraki, S. Fukatsu, Y. Shiraki, and R. Ito, Appl. Phys. Lett. **61**, 557 (1992).
[17]*Properties of Lattice-Matched and Strained Indium Gallium Arsenide*, Pallab Bhattacharya, Data Review Vol. 8 (INSPEC, London, 1993).
[18]C. Rivera, U. Jahn, T. Flissikowski, J. L. Pau, E. Muñoz, and H. T. Grahn, Phys. Rev. B **75**, 045316 (2007).